Ocean Engng, Vol. 14, No 5, pp. 409–433, 1987.
Printed in Great Britain.

0029–8018/87 $3.00 + .00

TURBIDITY CURRENTS ON STEEP SLOPES: APPLICATION OF AN AVALANCHE-TYPE NUMERIC MODEL FOR OCEAN THERMAL ENERGY CONVERSION DESIGN

A. T. DENGLER, JR and P. WILDE
Marine Sciences Group, Department of Paleontology, University of California, Berkeley, CA 94720, U.S.A.

Abstract—To minimize cold water pipe lengths, the most favorable land or fixed platform based Ocean Thermal Energy Conversions (OTEC) sites have subbottom slopes greater than 5°. Observations at OTEC sites in Hawaii indicate that turbidity currents of an impulsive or episodic nature can occur with frontal speeds of several meters per second. Such speeds and the attendant potential for sediment transport and abrasion along routes containing OTEC installations indicate that the pertinent features of these flows are an important design criteria for OTEC or any other steep-slope marine installation. To satisfy this need, models of oceanic turbidity flows and similar flows have been examined. The model that addresses OTEC steep-slope conditions most succinctly was developed originally by Hopfinger and Tochon-Danguy (1977) for snow avalanches on land. This two-dimensional avalanche model is used to estimate the speed and growth characteristics of potential turbidity currents downslope for various postulated marine conditions of initial flow density, height, volume, and length at slopes from 5 to 60°. The areas of additional research required to increase reliability of the analyses are in the initiation and initial development of a turbidity plume, the mechanisms of sediment entrainment to and loss from the plume, and three-dimensional in addition to two-dimensional studies.

INTRODUCTION

THIS RESEARCH is designed to evaluate the characteristics of turbidity/suspension currents that can occur at locations of interest for Ocean Thermal Energy Conversion (OTEC) facilities. Turbidity/suspension currents are a sub-class of density current where the driving force is due to density differences caused by suspended solids (clays, muds, etc.). Turbidity/suspension currents generally are natural phenomena and episodic in occurrence. The potential for turbidity/suspension currents at sites of interest for OTEC is recognized from the study of Normark *et al.* (1982) that examined sediments and bathymetry at the OTEC 40MW Pilot Plant site off Kahe Point, Oahu, Hawaii, and the analyses of Dengler *et al.* (1984a,b) that reported on the actual observations, at the same site, of a turbidity current that appeared to have been initiated by associated effects of a passing hurricane, Iwa. The immediate concern for OTEC is that bottom mounted installations (pipelines, cables, foundations, moorings), could be damaged or destroyed by turbidity/suspension current events.

OTEC systems have two properties that predispose them toward locations with steep slopes and therefore toward risk of turbidity/suspension currents. The first is that many of the islands that are within the area where the ocean thermal resource is sufficient for OTEC power generation are of volcanic origin and exhibit steep slopes in the surrounding bathymetry (Chase *et al.*, 1986). The second is that the length and, to a large degree, the cost of the pipeline necessary to reach the cold water resource are less when steeper bathymetry can be followed (Lewis *et al.*, 1985).

The importance of knowledge of turbidity/suspension currents for design has been recognized in the design of the pipe system for the 40-MW OTEC Pilot Plant at Kahe Point, Oahu, Hawaii (OTC, 1984). The rough estimates of speed, direction and sediment concentration developed by Dengler *et al.* (1984a,b) were used by R. J. Brown, Inc. to provide limits on the conditions that the pipeline would need to survive after installation. The Steep-Slope Numeric Program is designed to provide the engineers with estimates of the characteristics of turbidity currents that might be expected at OTEC sites.

The approach taken is to identify, from published literature and experts in field, the present state-of-art turbidity/suspension current numeric models. Appropriate test candidates can then be selected from the identified models. The criteria for selection are: boundary conditions sufficiently flexible to encompass potential OTEC; parameters (slopes, volume concentration of sediment, Froude numbers, Reynolds numbers, Richardson numbers, thickness of flow, entrainment coefficient, sediment density, velocity) appropriate for ranges of OTEC variables; separation of dependent and independent variables possible for variables of importance for OTEC design (drag coefficients, flow thickness, bed shear stress); formulae that can be numerically coded; and scalability of model results to OTEC time and space scales. Ranges of available parameters most appropriate for OTEC applications are defined for use as independent variables in the model simulations. The simulations are run over defined ranges of parameters and with specified boundary conditions to obtain the responses of dependent variables. Finally, the results (plots and tabulated values of dependent variables vs independent variables) are interpreted for use in evaluating designs for OTEC structures.

DESCRIPTION OF TURBIDITY CURRENTS

Definitions of turbidity and density currents

Turbidity currents are a subclass of the broader category of density currents. Density currents also are termed gravity currents. A density current "is the flow of one fluid within another caused by the density difference between the fluids. The difference in specific weight that provides the driving force may be due to dissolved or suspended material or to temperature differences" (Simpson, 1982). Turbidity currents exist when the density difference is due to suspended sediment and, of course, the fluids involved are both water.

Examples of density currents

Density currents occur in many forms in nature. Examples of density currents in lakes and seas are: cold river inflows at the warmer surface of lakes and reservoirs; saline outflow of evaporative basins into less saline bodies, such as the outflow of the Mediterranean basin into the Atlantic through the Straits of Gibraltar; and, the formation of cold dense water on polar shelves that then sinks to form deep ocean water. At the land-atmosphere boundary, density currents include several types of catastrophic phenomena: avalanches; mudslides; nuées ardentes (gas and ash flows) and lahars (mud and melted snow and ice flows) associated with volcanoes. In the atmosphere, density current phenomean include: catabatic drainage winds from plateau (such as the "bora", "mistral", and "Santa Ana" winds; sea breeze flows; thunderstorm base flows (wind shear); and, manmade smokestack discharges).

Marine observations of turbidity currents

Dengler *et al.* (1984a) observed that "Current measurements on coastal slopes and in submarine canyons have resulted in an increasing number of observations of low-speed turbidity currents. Although current or wave event speeds as high as 750 cm/sec, calculated from cable breaks following the 1929 Grand Banks earthquake, appear possible (Shepard, 1963), actual measurements in submarine canyons show lower water current speeds of 50–70 cm/sec to be more common (Shepard *et al.*, 1977; Shepard and Marshall, 1978). Current speeds as high as 190 cm/sec have been observed (Inman *et al.*, 1976), and speeds of 200–250 cm/sec have been estimated from submersible observation (Keller and Shepard, 1978). All but one of the submarine canyons where turbidity currents have been observed are at the mouths of rivers where large quantities of sediment are discharged. The turbidity current speeds are sufficient to suspend and transport sediment (Middleton and Hampton, 1976; Miller *et al.*, 1977), and sediment has been deposited on the current sensors (Shepard *et al.*, 1977; Shepard *et al.*, 1975; Lambert *et al.*, 1976)."

Initiation of marine turbidity currents

A number of phenomena have been implicated in the initiation of turbidity currents. Dengler *et al.*, (1984a) observed that "The initiation of low-speed turbidity currents have been linked to surface waves (Shepard *et al.*, 1975; Reimnitz, 1971), winds (Inman *et al.*, 1976; Shepard and Marshall, 1973), and storm surges in rivers (Lambert *et al.*, 1976; Gennesseaux *et al.*, 1971) that resuspend or destabilize accumulated sediment. The sediment and water then form a suspension that cascades down the canyon slopes."

Description of an observed turbidity current

Limited observations of real turbidity currents make it difficult to develop a physical sense of the phenomenon. Most observations are *a-postiori* examinations of the results of turbidity currents; for example, estimation of current velocity from grain size (Wilde, 1965). The most extensive *in-situ* observations are of a turbidity current that occurred at a site of interest for OTEC applications, from Dengler *et al.* (1984b). "On November 23, 1982, during the passage of hurricane Iwa, current sensor moorings in place along the proposed pipe-line route for the Ocean Thermal Energy Conversion (OTEC) Pilot Plant at Kahe Point, Oahu, Hawaii, moved downslope during a sequence of slump and/or turbidity current events (Fig. 1). Moorings were initially situated between 100 and 760 m water depth within a 4-km wide re-entrant of the submarine volcanic slope. Sensors recorded total depth changes, during at least four events, of as much as 220 m, implying downslope movement of as much as 2.4 km. The downslope movement occurred as a series of episodes that could be traced sequentially through the series of moorings. Episodes of downslope movement were associated with a rapid increase in near-bottom current speed of up to 220 cm/sec. Temperature of 2–4°C above ambient indicates that the sources for the water in the downslope current are several hundred

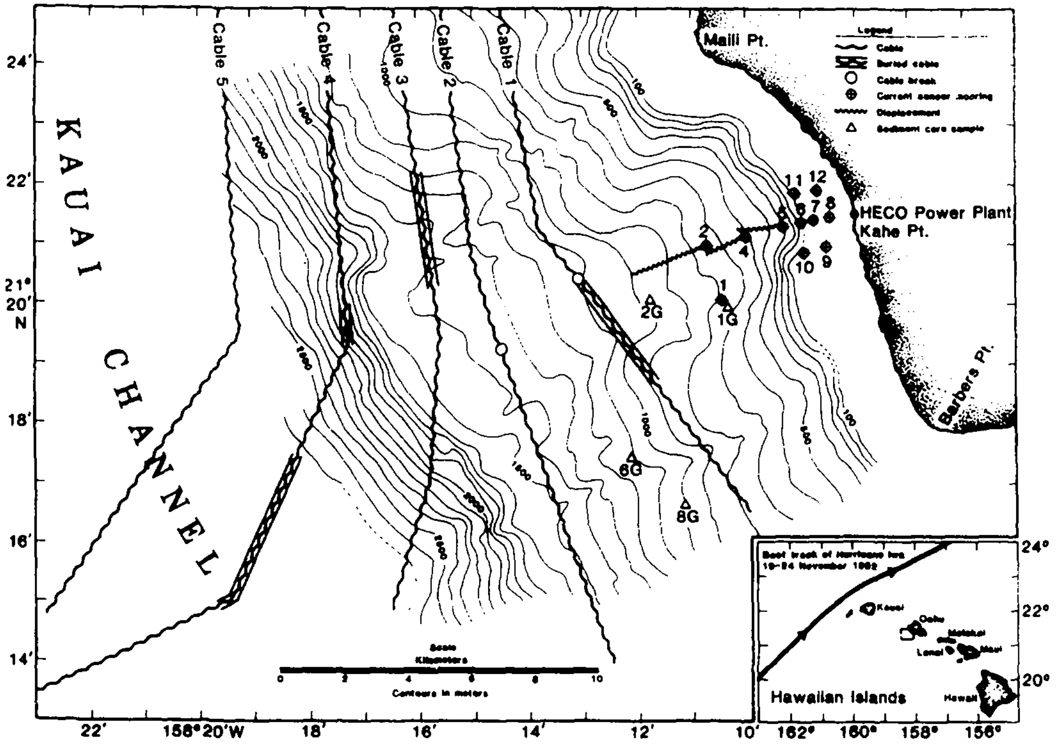

FIG. 1. Bathymetric map of area off Kahe Point, Oahu, Hawaii studied as a site for an OTEC Pilot Plant. A turbidity current was observed at the site on 23 November 1982 as the eye of hurricane Iwa passed about 150 km to the northwest. Submarine cables that broke or showed damage are shown, as well as the array of current sensor moorings that recorded extreme currents and/or were displaced downslope by the turbidity current (Dengler *et al.*, 1984a,b).

meters above the initial position of each sensor. At least four specific events, which we interpret at turbidity currents, can be recognized in a 2 h period. The arrival times at successive sensors indicate a downslope speed of 300 cm/sec for the events. Communication cables in water depths of 1100 – 2000 m exhibited breaks or damage concurrent with the turbidity flow."

SURVEY OF MODELS

A number of theoretical and experimental models have been developed to address the phenomenon of density currents. Simpson (1982) offers a general review of research performed in the area of gravity currents in laboratory, atmosphere, and ocean environments. Of most interest for OTEC situations are examinations of gravity currents on slopes and of suspension flows. These studies can be divided into two regimes; shallow slopes from 0 to 5°, and steep slopes from 5 to 90°. A simplifying constraint on work in this field is that all of the available studies address two-dimensional currents. Therefore, the present analysis is similarly constrained.

Behavior of density currents on shallow slopes has been subject of several experimental analyses. Middleton (1966 a, b, c) studied the advance of the head of a saline gravity current down a gently sloping (less than 5°) two-dimensional channel, building on Keulegan's (1957, 1958) lock exchange work on saline gravity surges in freshwater channels. Komar (1977) extended these results theoretically to two-dimensional turbidity currents on low slopes. The findings of these investigators have been used in an *a-posteriori* study by Bowen *et al.* (1984) to determine the nature of an earlier turbidity current from channel morphology and sediment thickness and grain size in the Navy Submarine Fan off the California coast.

The work on gravity currents on steep slopes can be divided further into three classes; continuous plumes, starting plumes, and thermal plumes or finite surges. Ellison and Turner (1959) studied the behavior of a continuous two-dimensional plume on slopes varying from 12 to 90°. They evaluated the entrainment of ambient fluid into the plume and found entrainment to be dependent upon the velocity of the layer and the Richardson number, determined from the buoyancy flux and the dimensions of the plume. Tochon-Danguy and Hopfinger (1975) performed further experiments with continuous plumes, measuring frontal velocity and characteristics of the head, and included the possibility of the flow entraining additional material in its path. Frontal velocity increased with increasing inflow rate and was roughly independent of slope, and rate of head growth increased with increasing inflow rate and slope.

Experiments with starting plumes from continuous sources were performed by Britter and Simpson (1978) on level slopes and by Britter and Linden (1980) on inclines. They found that frontal velocity was proportional to the cube root of the buoyancy flux at the source. Hay (1983) was able to reproduce theoretically these experimentally determined frontal velocities.

Thermal plumes, or instantaneously released flows, have been addressed in two studies. The first, by Hopfinger and Tochon-Danguy (1977), in a principally theoretical examination, studied speeds and growth of a thermal plume with the potential for entrainment of additional dense material by the plume from its path. The second, by Beghin *et al.* (1981), is an experimental analysis of frontal velocities and rates of growth of two-dimensional plumes on steep slopes. They find that, in a thermal plume without entrainment of material in its path, the frontal velocity decreases with distance from the source, due to entrainment of ambient fluid and enlargement of the thermal. At low slopes, less than 5°, a thermal plume becomes increasingly like a continuous gravity plume. Conversely, when the continuous source of a starting plume is removed, the plume development with time will correspond increasingly to a thermal.

SELECTED MODEL

For OTEC interests, there is concern with steep-slopes of greater than 5°, and the type of gravity flow anticipated and observed corresponds to the thermal plume. Also, we can anticipate the possibility of entraining sediment into the plume from along the path of the plume. For these reasons, we have selected the Avalanche model outlined by Hopfinger and Tochon-Danguy (1977) for examination. As noted above, their model exhibits the appropriate set of features.

General description

The Avalanche model treats the flow of a finite volume of dense fluid down a slope. The flow may entrain additional dense material from a layer along its path. The speed and dimensions of the plume will vary with distance from the source, amount of dense material initially at the source and entrained from the path, and the slope. Speed increases with increasing dense material in the plume and slightly with the slope, and decreases with distance downslope. Size increases with source size, distance downslope, and the slope itself. The amount of material entrained along the path is a constant fraction of the material available on the path. Throughout its development, the theoretical plume maintains a similar profile of approximately an half-ellipse, although in reality, we can anticipate a wake developing behind the plume, especially when the plume is a turbidity current and the density difference is due to sediment (Beghin *et al.*, 1981).

Assumptions and limitations

In order to keep the phenomenon of turbidity currents tractable with this straightforward technique, a number of assumptions must be incorporated into the Avalanche model. The first assumption requires the previously stated two-dimensional simplification. This assumption is necessary due to the status of work in this field, and it will be reasonable whenever the flow is constrained to a channel or canyon. When flow is unconstrained by lateral boundaries, the violation of this assumption will have uncertain effects. A second assumption is that the density of the plume is approximately equal to the density of the ambient fluid. This second assumption is reasonable and we do not expect it to be violated for turbidity currents (Bagnold, 1962). A third assumption is of a simplified entrainment process for sediment along the path of the turbidity current. In the model the amount of sediment entrained is proportional to the thickness of the available sediment layer, and must be only a small fraction of the sediment load in the plume. In practice, the entrained sediment should be related to the particle-size distribution of the sediment and the speed, size, and duration of the turbidity current and should be limited to the available sediment layer. Correction of this simplified sediment entrainment process is an appropriate topic for further research. A fourth assumption is that there is no loss of sediment from the turbidity either to a wake or through settling. In the model, the potential for loss of sediment may be adjusted into the along path entrainment, but an accurate treatment of these losses is as yet an unaddressed problem. For the steep slopes likely to be encountered in OTEC development, the no-sediment loss assumption is reasonable. A fifth assumption is that the plume is fully developed from its inception, with the appropriate dimensions, characteristics and velocity. Finally, the model applies to slopes greater than 5°. At less than 5°, drag at the bottom of the turbidity current becomes relatively more important, and the thermal plume nature of the turbidity current grades into a continuous starting plume structure as modeled by Britter and Simpson (1978).

Variables

Figure 2 shows a reference sketch of an inclined thermal and the associated variables (Hopfinger and Tochon-Danguy, 1977). The following is a list of variables used in the model.

$A \quad \propto HL$ = volume per unit width

$A_0 \quad \propto (H_0)(L_0)$

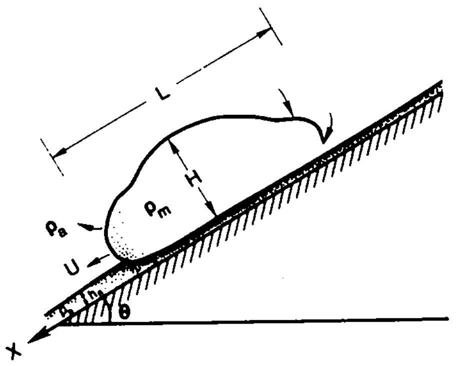

FIG. 2. Definition sketch of thermal (impulsive) turbidity plume (Hopfinger and Tochon-Danguy, 1977). L = length along direction of travel; H = height normal to direction of travel; ρ_m = mean density of plume; ρ_a = ambient density of the surrounding fluid: ρ_n = density of sediment along path of flow; h_n = depth of sediment along path; U = frontal speed; X = direction of travel; θ = angle of slope.

C = experimentally determined constant
C_1 = experimentally determined constant
C_2 = theoretically determined constant
E = experimentally determined entrainment constant
g = acceleration due to gravity
H = height normal to direction of travel
H_0 = initial height
h_n = depth of sediment on path
L = length along direction of travel
L_0 = initial length
ρ_a = ambient density
ρ_m = mean density of plume
ρ_n = density of sediment in path
ρ_0 = initial density of plume
$\Delta\rho_m$ = $\rho_m - \rho_a$
$\Delta\rho_n$ = $\rho_n - \rho_a$
$\Delta\rho_0$ = $\rho_0 - \rho_a$
S = shape factor
θ = slope angle
U = frontal speed
U_0 = initial speed of turbidity
V_0 = initial volume of sediment available for turbidity
X = direction of travel
x = distance travelled from virtual origin
x_0 = initial position
Z = direction normal to direction of travel
z = distance normal to direction of travel.

Algorithms

The equations governing the model are listed below:
The experimentally determined fluid entrainment factor is

$$E = 3(10^{-3})\,(5+\theta). \tag{1}$$

The height of the plume as a function of distance traveled is

$$H = E(x). \tag{2}$$

The cross sectional area of the plume is

$$A = SH^2 \tag{3}$$

where shape factor, given that the plume is an half-ellipse, is

$$S = (1/4)\,\pi. \tag{4}$$

The initial height of the plume is

$$H_0 = (A_0/S)^{1/2}, \tag{5}$$

the initial position of the plume is

$$x_0 = H_0/E,\, x_0>0, \tag{6}$$

and the initial cross section of the plume is

$$A_0 = V_0(\Delta\rho_n)/(\Delta\rho_0),\, A_0 \geqq V_0\,. \tag{7}$$

The frontal speed is then

$$U = C[(g(1/\rho_m E)\,(sin\;\theta)\,(C_2\Delta\rho_n h_n + \Delta\rho_0 A_0/x)]^{1/2},\, x>0. \tag{8}$$

Substituting Equations (5), (6) and (7) into Equation (8), and setting $h_n = 0$,

$$U_0 = C[g(1/\rho_m)(sin\;\theta)]^{1/2}[V_0\Delta\rho_n\Delta\rho_0]^{1/4} \tag{9}$$

C is experimentally determined as

$$C = 2$$

and C_z assumed to be,

$$C_2 = 1$$

for cases where sediment in the path will be eroded and

$$C_2 = 0 \text{ otherwise.}$$

For turbidity currents, ρ_m in Equations (8) and (9) may be approximated as 1 with only slight loss of accuracy.

Guide to use of algorithms

For the level of prediction available from this model, we can specify several steps to follow to obtain the impressionistic estimate of the turbidity current that could occur at a given site.

(1) From surveys of the site, estimate bottom slope, θ, volume of sediment per unit width, V_0, available for initiation of turbidity currents, and depth of sediment, h_n, available for entrainment along the path of the turbidity.

(2) Calculate, from V_0, the possible ranges of initial size, A_0, density, ρ_0, and $A_0 \rho_0$, using Equation (7), or Fig. A1.

(3) From θ, calculate E, using Equation (1).

(4) From range of A_0 estimate corresponding H_0 using Equation (5), or Fig. A2.

(5) From H_0, estimate x_0 using Equation (6), or Fig. A4.

(6) Calculate U_0 using Equation (9), or Figs A5 and A7.

(7) Using an independent method and estimates for H_0 and U_0, evaluate whether sediment in path of turbidity will erode.

(8) If sediment will not erode, calculate $U(x,A_0\rho_0,\theta)$, setting $C_2 = 0$, using Equation (8), or Appendix, Figs A8–A14.

(9) If sediment will erode, calculate $U(h_n,\theta)$, for x large, $(1/x) \approx 0$, using Equation (8), or Fig. A6.

(10) Calculate $H(x)$ from Equation (2), Fig. A3.

Following these steps, we will obtain estimates for speed and size of the turbidity current verses distance downslope, for different slopes, initial sizes, and depths of entrainable sediment in the path.

Future work

Several possibilities present themselves for direct extension of this analysis. The most straightforward possibility is to incorporate the work of Beghin *et al.* (1981) to allow a relaxation of the assumption that the turbidity current thermal is initially in motion at the appropriate speed. A pair of recent studies (Pantin, 1979; Parker, 1982) have addressed part of the problem of the ability of turbidity currents to erode and entrain sediments along the path, and thereby to sustain motion. Analysis of these studies may allow for more realistic evaluation of bed entrainment and results might be obtainable in a near-term (1 – 2 yr) research effort.

A pair of more distant research goals also present themselves. The first goal would be to understand the mechanisms for loss of sediment from the turbidity current. The two principal mechanism for loss are: (1) sedimentation of grains within and at the edges of the turbidity current and (2) loss of plume body to a wake behind the thermal plume. The second research effort would be to create a body of theoretical and experimental results using three-dimensional analyses.

Acknowledgements—The authors would like to thank Dr L. F. Lewis of the Department of Energy and Mr B. Shelpuk of Solar Energy Research Laboratory for their encouragement and support. M. Krup did her usual outstanding job in preparing the figures and preparing the manuscript for publication. This work was sponsored by the Department of Energy, Solar Energy Research Laboratory contract #XX-5-05000-1 and is contribution MSG-87-001 of the Marine Sciences Group of the University of California, Berkeley.

REFERENCES

Bagnold, R.A. 1962. Auto-suspension of transported sediment turbidity currents. *Proc. R. Soc.* **265**, A 315–319.

Bagnold, R.A. 1966. An approach to the sediment transport problem from general physics. U.S. Geol. Surv. Prof. Paper 422-I, p. 37.

Beghin, P., Hopfinger, E.J. and Britter, R.E. 1981. Gravitational convection from instantaneous sources on inclined boundaries. *J. Fluid Mech.* **107**, 407–422.

Bowen, A.J., Normark, W.R. and Piper, D.J.W. 1984. Modelling of turbidity currents on Navy Submarine Fan, California Continental Borderland. *Sedimentology* **31**, 169–185.

Britter, R.E. and Linden, P.F. 1980. The motion of the front of a gravity current travelling down an incline. *J. Fluid Mech.* **99**, 531–543.

Britter, R.E. and Simpson, J.E. 1978. Experiments on the dynamics of a gravity current head. *J. Fluid Mech.* **88**, 223–240.

Buffington, E.C. 1961. Experimental turbidity currents on the sea floor. *Am. Ass. Petrol. Geol. Bull.* **45**, 1392–1400.

Chase, T.E., Seekins, B.A., Wahler, J.A., Normark, W.R., Wilde, P. and Schwab, W.C. 1986. Geographic, Bathymetric, Geologic, and Physical Oceanographic data of Potential OTEC sites. Marine Sciences Group Publication 86–011, University of California, Berkeley, California, 2 sheets.

Chu, F.H., Pilkey, W.D. and Pilkey, O.H. 1979. An analytical study of turbidity current steady flow. *Mar. Geol.* **33**, 205–220.

Dengler, A.T., Wilde, P., Noda, E.K. and Normark, W.R. 1984a. Turbidity currents generated by hurricane Iwa. *Geo-Mar. Lett.* **4**, 5–11.

Dengler, A.T., Noda, E.K., Wilde, P. and Normark, W.R. 1984b. Slumping and related turbidity currents along proposed OTEC cold-water-pipe route resulting from hurricane Iwa. *Proc. Offshore Technology Conf, Houston, Texas*, 7–9 May 1984, Vol. **1**, pp. 475–480.

Ellison, T.H. and Turner, J.S. 1959. Turbulent entrainment in stratified flows. *J. Fluid Mech.* **6**, 432–448.

Gennesseaux, M., Guibout, P. and Lacombe, H. 1971. Enregistrement de courants de turbidité dans la Vallée Sous-Marine du Var (Alpes-Maritimes). *C. Rebd. Séanc. Acad. Sci., Paris* **273 D**, 2456–2459.

Hopfinger, E.J. and Beghin, P. 1980. Buoyant clouds appreciably heavier than the ambient fluid on sloping boundaries. *Second Int. Symp. on Stratified Flows, Norwegian Institute of Technology, Trondheim, Norway*, 24–27 June 1980, pp. 495–504.

Hopfinger, E.J. and Tochon-Danguy, J.-C. 1977. A model study of powder-snow avalanches. *J. Glaciol.* **19**, 343–356.

Inman, D.L., Nordstrom, C.E. and Flick, R.E. 1976. Currents in submarine canyons: an air–sea–land interaction. *Ann. Rev. Fluid Mech.* **8**, 275–310.

Keller, G.H. and Shepard, F.P. 1978. Currents and sedimentary processes in submarine canyons off the northeast United States. In *Sedimentation and Submarine Canyons, Fans and Trenches*, pp. 15–32. Edited by Stanley, D.J. and Kelling, G. Dowden, Hutchinson & Ross, Stroudsburg, PA.

Keulegan, G.H. 1957. An experimental study of the motion of saline water from locks into fresh water channels. U. S. Nat. Bur. Stand., Rept 5168.

Keulegan, G.H. 1958. The motion of saline fronts in still water. U.S. Nat. Bur. Stand., Rept 5831.

Komar, P.D. 1969. The channelized flow of turbidity currents with application to Monterey deep-sea fan channel. *J. geophys. Res.* **74**, 4544–4558.

Komar, P.D. 1977. Computer simulation of turbidity current flow and the study of deep-sea channels and fan sedimentation. In: *The Sea: Ideas and Observations on Progress in the Study of the Sea*, pp. 603–621. Edited by Goldberg, E.D. Wiley, New York, NY.

Lambert, A.M., Kelts, D.R. and Marshall, N.F. 1976. Measurements of density underflows from Walensee, Switzerland. *Sediment.*, **23**, 87–105.

Lewis, L.F., Quinby-Hunt, M.S. and Wilde, P. 1985. Environmental Assessment: A Tool for Engineers. *Oceans85* **1**, 27–32.

Middleton, G.V. 1966a. Experiments on density and turbidity currents. I. Motion of the head. *Can. J. Earth Sci.* **3**, 523–546.

Middleton, G.V. 1966b. Experiments on density and turbidity currents. II. Uniform flow of density currents. *Can. J. Earth Sci.* **3**, 627–637.

Middleton, G.V. 1966c. Small-scale models of turbidity currents and the criterion for auto-suspension. *J. Sed. Pet.* **36**, 202–208.

Middleton, G.V. and Hampton, M.A. 1976. Subaqueous sediment transport and deposition by sediment gravity flows. In *Marine Sediment Transport and Environmental Management*, pp. 197–218. Edited by Stanley, D.J. and Smith, D.J.P. Wiley Interscience, New York.

Miller, M.C., McCave, I.N. and Komar, P.D. 1977. Threshold of sediment motion under unidirectional currents. *Sediment.* **24**, 507–527.

Normark, W.R., Chase, T.E., Wilde, P., Hampton, M.A., Gutmacher, C.E., Seekins, B.A. and Johnson, K.H. 1982. Geologic report for the O'OTEC site off Kahe Point, Oahu, Hawaii. U. S. Geol. Sur. Open File Rept. 82–468A, p. 32.

Pantin, H.M. 1979. Interaction between velocity and effective density in turbidity flow. Phase-plane analysis, with criteria for autosuspension. *Mar. Geol.* **31**, 59–99.

PARKER, G. 1982. Conditions for the ignition of catastrophically erosive turbidity currents. *Mar. Geol.* **46**, 307–327.

REIMNITZ, E. 1971. Surf-beat origin for pulsating bottom currents in the Rio Balsas Submarine Canyon, Mexico. *Bull. geol. Soc. Am.* **83**, 81–90.

SANDERS, J.E. 1963. Concepts of fluid mechanics provided by primary sedimentary structures. *J. Sed. Pet.* **33**, 173–179.

SHEPARD, F.P. 1963. *Submarine Geology*, 2nd edn, p. 577. Harper and Row, New York.

SHEPARD, F.P. and MARSHALL, N.F. 1973. Storm generated current in La Jolla Submarine Canyon, California. *Mar. Geol.* **15**, M19–M24.

SHEPARD, F.P. and MARSHALL, N.F. 1978. Currents in submarine canyons and other sea valleys. In: *Sedimentation and Submarine Canyons. Fans and Trenches*, pp. 1–14. Edited by STANLEY, D.J. and KELLING, G. Dowden, Hutchinson & Ross, Stroudberg, PA.

SHEPARD, F.P., MARSHALL, N.F. and MCLOUGHLIN P.A. 1975. Pulsating turbidity currents with relationship to high swell and high tides. *Nature, Lond.* **258**, 704–706.

SHEPARD, F.P., MCLOUGHLIN, P.A., MARSHALL, N.F. and SULLIVAN, G.C. 1977. Current meter recordings of low speed turbidity currents. *Geol.* **5**, 297–301.

SIMPSON, J.E. 1982. Gravity currents in the laboratory, atmosphere and ocean. *Ann. Rev. Fluid Mech.* **14**, 213–234.

SMITH, J.D. 1977. Modelling of sediment transport on continental shelves. *The Sea* **6**, 539–577.

TOCHON-DANGUY, J.-C. and HOPFINGER, E.H. 1975. Simulation of the dynamics of powder avalanches. *Proc. Grindelwald Symp.*, April 1974. IAHS-AISH Publication No. 114, pp. 369–380.

WILDE, P. 1965. Estimates of bottom current velocities from grain-size measurements from the Monterey deep-sea fan. *Proc. Mar. Tech. Soc.–Am. Lit.* **2**, 718–727.

APPENDIX A—AVALANCHE MODEL CALCULATIONS

This model is designed to calculate the speed and growth of a turbidity current with distance downslope. It allows for additional entrainment of sediment in the path and treats the current as a 2-d thermal pulse. The model assumes:

- ambient density and plume density are approximately equal,
- entrained sediment is a small fraction of plume sediment,
- entrained sediment is a constant fraction of available sediment,
- slope is greater than 5 degrees so that bottom drag can be ignored,
- there is no loss of entrained sediment.

The following figures with tabular data give a sample set of calculations for a realistic marine case. The list of variables are defined as given in the main text. For a detailed analysis and discussion of the mathematical basis of the model, the reader is referred to Hopfinger and Tochon-Danguy (1977, pp. 343–356).

Values for parameters

$C = 2$
$C_2 = 1$
$g = 10\ \mathrm{m/sec^2}$
$\rho_a = 1\ \mathrm{kg/m^3}$
$\rho_n = 2.7\ \mathrm{kg/m^3}$
$\Delta\rho_n = 1.7\ \mathrm{kg/m^3}$
$S = 0.78539$
$H = Ex$
$A = SH^2$
$E = 310^{-3}(5+S)$
$U \quad C[g(1/\rho_m E)(\sin\theta)((C_2\Delta\rho_n h_n) + (\Delta\rho_0 A_0/x))]^{.5}$.

Initial steps (also see in main text *Guide to use of Algorithms*):

(1). Determine initial amount of sediment available $= V_0$.
(2). Estimate range of densities ρ_0 of the plume.
(3). Calculate initial volume per unit length, A_0 where:

$$\Delta\rho_n V_0 = \Delta\rho_0 A_0 .$$

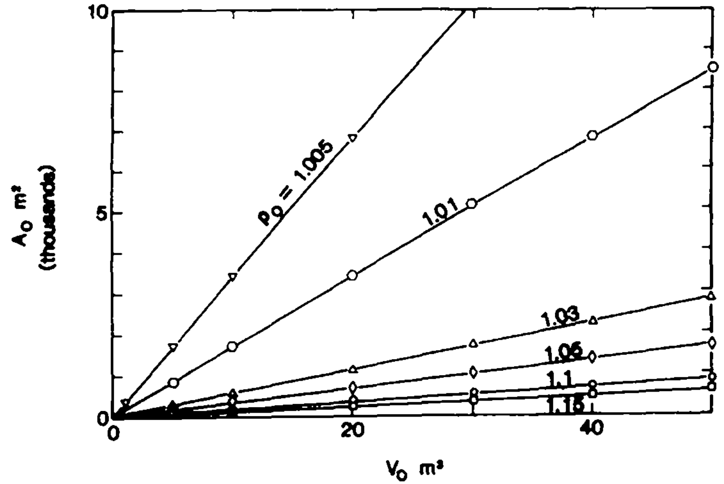

FIG. A1. Initial volume per unit width, A_0, as a function of V_0 for various ρ_0.

ρ_0 =	1.15	1.1	1.05	1.03	1.01	1.005
V_0 in m³	A_0 in m²					
0.5	5.7	8.5	17	28.3	85	170
1	11.3	17.0	34	56.7	170	340
5	56.7	85.0	170	283.3	850	1700
10	113.3	170.0	340	566.7	1700	3400
20	226.7	340.0	680	1133.3	3400	6800
30	340.0	510.0	1020	1700.0	5100	10200
40	453.3	680.0	1360	2266.7	6800	13600
50	566.7	850.0	1700	2833.3	8500	17000

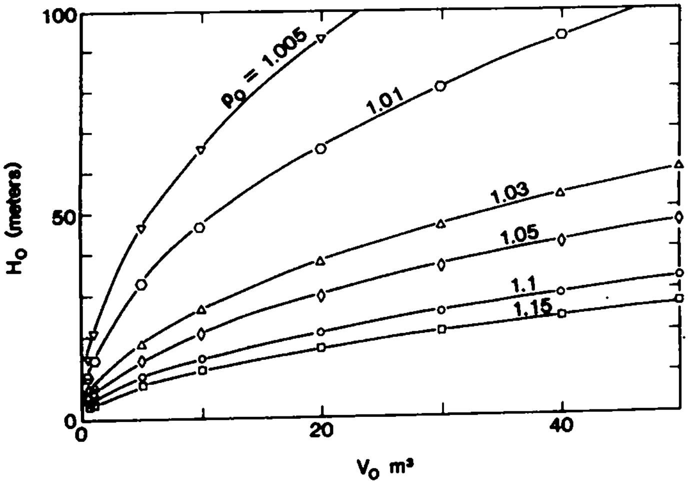

FIG. A2. Initial height of plume, H_0, as a function of V_0 for various ρ_0.

ρ_0 =	1.15	1.1	1.05	1.03	1.01	1.005
V_0 in m³	H_0 in m					
0.5	2.7	3.3	4.7	6.0	10.4	14.7
1.0	3.8	4.7	6.6	8.5	14.7	20.8
5.0	8.5	10.4	14.7	19.0	32.9	46.5
10.0	12.0	14.7	20.8	26.9	46.5	65.8
20.0	17.0	20.8	29.4	38.0	65.8	93.0
30.0	20.8	25.5	36.0	46.5	80.6	114.0
40.0	24.0	29.4	41.6	53.7	93.0	131.6
50.0	26.9	32.9	46.5	60.1	104.0	147.1

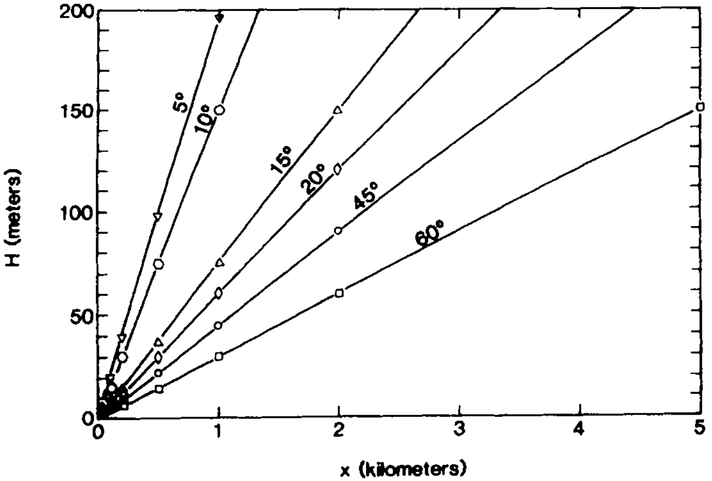

Fig. A3. Height of plume, H, as a function of distance traveled, x, for various slopes, θ.

θ =	5°	10°	15°	20°	45°	60°	90°
E =	0.03	0.045	0.06	0.075	0.15	0.195	0.285
x in m	H in m						
10	0.30	0.45	0.60	0.75	1.50	1.95	2.85
20	0.60	0.90	1.20	1.50	3.00	3.90	5.70
50	1.50	2.25	3.00	3.75	7.50	9.75	14.25
100	3.00	4.50	6.00	7.50	15.00	19.50	28.50
200	6.00	9.00	12.00	15.00	30.00	39.00	57.00
500	15.00	22.50	30.00	37.50	75.00	97.50	142.50
1000	30.00	45.00	60.00	75.00	150.00	195.00	285.00
2000	60.00	90.00	120.00	150.00	300.00	390.00	570.00
5000	150.00	225.00	300.00	375.00	750.00	975.00	1425.00

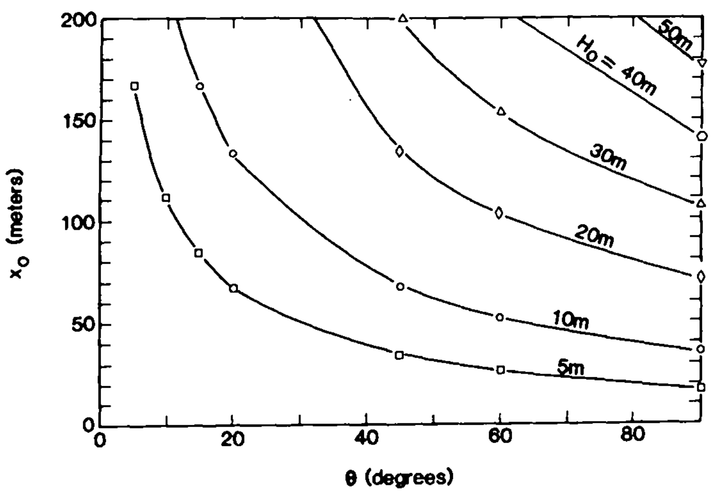

FIG. A4. Initial position, x_0, as a function of slope θ, for various initial height, H_0.

θ =	5°	10°	15°	20°	45°	60°	90°
E =	0.03	0.045	0.06	0.075	0.15	0.195	0.285
H_0 in m	x_0 in m						
5	167	111	83	67	33	26	18
10	333	222	167	133	67	51	35
20	667	444	333	267	133	103	70
30	1000	667	500	400	200	154	105
40	1333	889	667	533	267	205	140
50	1667	1111	833	667	333	256	175

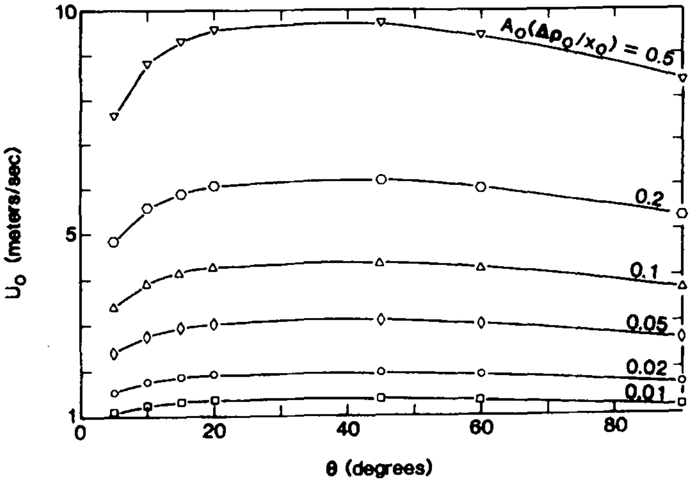

FIG. A5. Initial speed, U_0, as a function of slope θ, for various $A_0\Delta\rho_0/x_0$.

θ =	5°	10°	15°	20°	45°	60°	90°
$A_0\Delta\rho_0/x_0$	U_0 in m/sec						
0.01	1.1	1.2	1.3	1.4	1.4	1.3	1.2
0.02	1.5	1.8	1.9	1.9	1.9	1.9	1.7
0.05	2.4	2.8	2.9	3.0	3.1	3.0	2.6
0.1	3.4	3.9	4.2	4.3	4.3	4.2	3.7
0.2	4.8	5.6	5.9	6.0	6.1	6.0	5.3
0.5	7.6	8.8	9.3	9.6	9.7	9.4	8.4

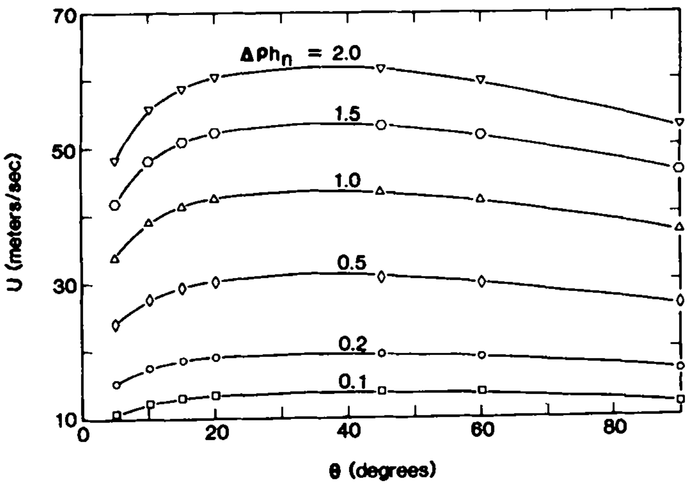

FIG. A6. Limit speed, U, as a function of slope θ, for various $\Delta\rho_n h_n$.

θ =	5°	10°	15°	20°	45°	60°	90°
$\Delta\rho_n h_n$	U in m/sec						
0.1	3.4	3.9	4.2	4.3	4.3	4.2	3.7
0.2	4.8	5.6	5.9	6.0	6.1	6.0	5.3
0.5	7.6	8.8	9.3	9.6	9.7	9.4	8.4
1	10.8	12.4	13.1	13.5	13.7	13.3	11.8
1.5	13.2	15.2	16.1	16.5	16.8	16.3	14.5
2	15.2	17.6	18.6	19.1	19.4	18.8	16.8

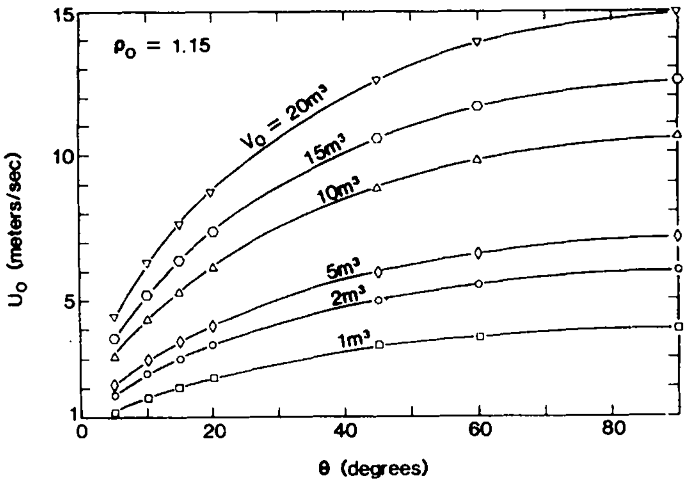

FIG. A7. Initial speed, U_0, as a function of slope θ, for various V_0. $\rho_0 = 1.15$ and V_0 proportional to $\Delta\rho_0^{.25}$.

θ =	5°	10°	15°	20°	45°	60°	90°
V_0 in m^3	U_0 in m/sec						
0.1	1.2	1.6	2.0	2.3	3.3	3.7	4.0
0.5	1.7	2.5	3.0	3.5	5.0	5.5	5.9
1	2.1	2.9	3.6	4.1	5.9	6.6	7.0
5	3.1	4.4	5.4	6.2	8.9	9.8	10.5
10	3.7	5.2	6.4	7.3	10.5	11.7	12.5
20	4.4	6.2	7.6	8.7	12.5	13.9	14.9

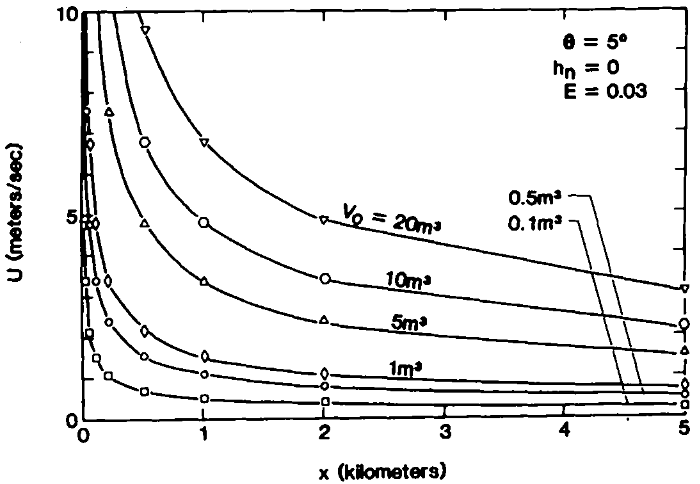

FIG. A8. Speed, U, as a function of distance, x, from virtual origin for various V_0 with $h_n = 0$, $\theta = 5°$, $E = 0.03$.

V_0 =	0.1	0.5	1	5	10	20
x in m	U in m/sec					
10	4.76	10.65	15.06	33.67	47.61	67.33
20	3.37	7.53	10.65	23.80	33.67	47.61
50	2.13	4.76	6.73	15.06	21.29	30.11
100	1.51	3.37	4.76	10.65	15.06	21.29
200	1.06	2.38	3.37	7.53	10.65	15.06
500	0.67	1.51	2.13	4.76	6.73	9.52
1000	0.48	1.06	1.51	3.37	4.76	6.73
2000	0.34	0.75	1.06	2.38	3.37	4.76
5000	0.21	0.48	0.67	1.51	2.13	3.01

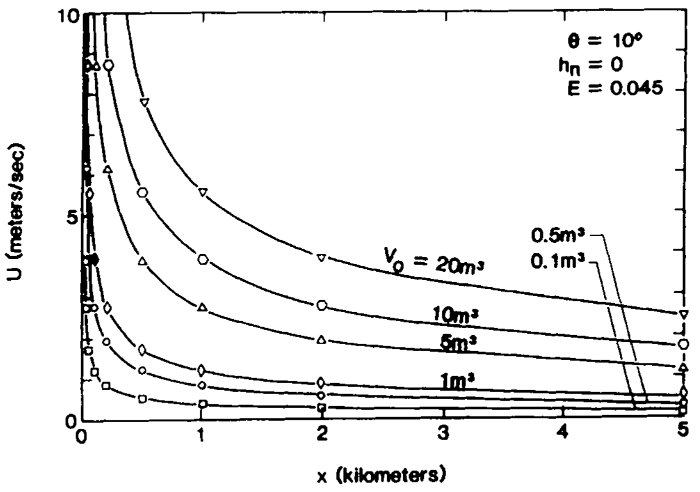

FIG. A9. Speed, U, as a function of distance, x, from virtual origin for various V_0 with $h_n = 0$, $\theta = 10°$, and $E = 0.045$.

V_0 =	0.1	0.5	1	5	10	20
x in m	U in m/sec					
10	3.89	8.69	12.29	27.49	38.87	54.97
20	2.75	6.15	8.69	19.44	27.49	38.87
50	1.74	3.89	5.50	12.29	17.38	24.59
100	1.23	2.75	3.89	8.69	12.29	17.38
200	0.87	1.94	2.75	6.15	8.69	12.29
500	0.55	1.23	1.74	3.89	5.50	7.77
1000	0.39	0.87	1.23	2.75	3.89	5.50
2000	0.27	0.61	0.87	1.94	2.75	3.89
5000	0.17	0.39	0.55	1.23	1.74	2.46

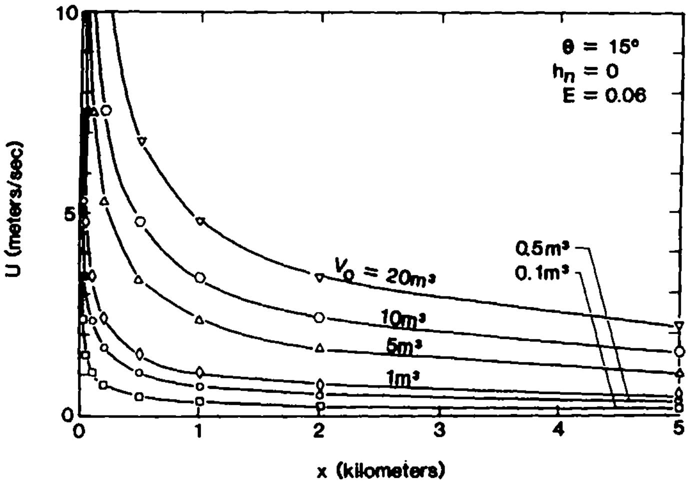

FIG. A10. Speed, U, as a function of distance, x, from virtual origin for various V_0 with $h_n = 0$, $\theta = 15°$, and $E = 0.06$.

V_0 =	0.1	0.5	1	5	10	20
x in m	U in m/sec					
10	3.37	7.53	10.65	23.80	33.67	47.61
20	2.38	5.32	7.53	16.83	23.80	33.67
50	1.51	3.37	4.76	10.65	15.06	21.29
100	1.06	2.38	3.37	7.53	10.65	15.06
200	0.75	1.68	2.38	5.32	7.53	10.65
500	0.48	1.06	1.51	3.37	4.76	6.73
1000	0.34	0.75	1.06	2.38	3.37	4.76
2000	0.24	0.53	0.75	1.68	2.38	3.37
5000	0.15	0.34	0.48	1.06	1.51	2.13

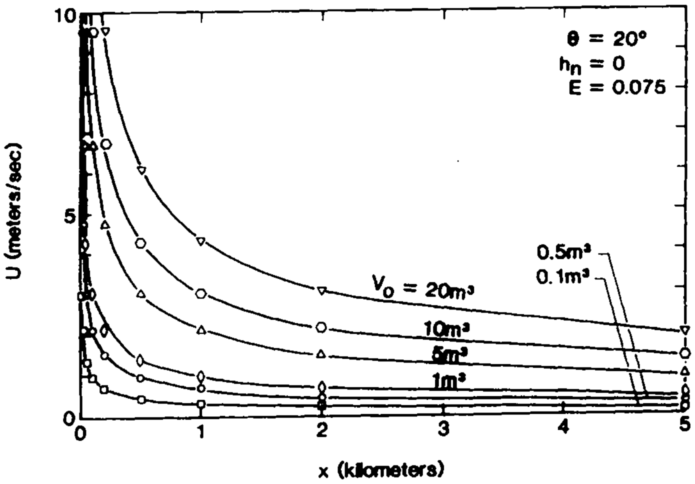

FIG. A11. Speed, U, as a function of distance, x, from virtual origin, for various V_0 with $h_n = 0$, $\theta = 20$, and $E = 0.075$.

V_0 =	0.1	0.5	1	5	10	20
x in m	U in m/sec					
10	3.01	6.73	9.52	21.29	30.11	42.58
20	2.13	4.76	6.73	15.06	21.29	30.11
50	1.35	3.01	4.26	9.52	13.47	19.04
100	0.95	2.13	3.01	6.73	9.52	13.47
200	0.67	1.51	2.13	4.76	6.73	9.52
500	0.43	0.95	1.35	3.01	4.26	6.02
1000	0.30	0.67	0.95	2.13	3.01	4.26
2000	0.21	0.48	0.67	1.51	2.13	3.01
5000	0.13	0.30	0.43	0.95	1.35	1.90

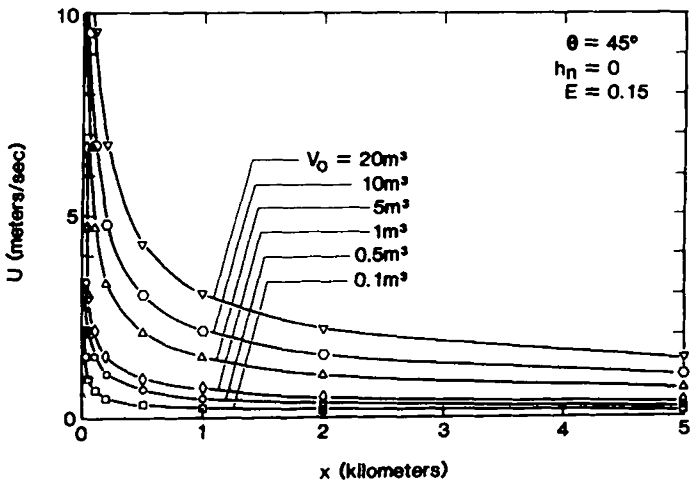

FIG. A12. Speed, U, as a function of distance, x, from virtual origin for various V_0 with $h_n = 0$, $\theta = 45°$, and $E = 0.15$.

V_0 =	0.1	0.5	1	5	10	20
x in m	U in m/sec					
10	2.13	4.76	6.73	15.06	21.29	30.11
20	1.51	3.37	4.76	10.65	15.06	21.29
50	0.95	2.13	3.01	6.73	9.52	13.47
100	0.67	1.51	2.13	4.76	6.73	9.52
200	0.48	1.06	1.51	3.37	4.76	6.73
500	0.30	0.67	0.95	2.13	3.01	4.26
1000	0.21	0.48	0.67	1.51	2.13	3.01
2000	0.15	0.34	0.48	1.06	1.51	2.13
5000	0.10	0.21	0.30	0.67	0.95	1.35

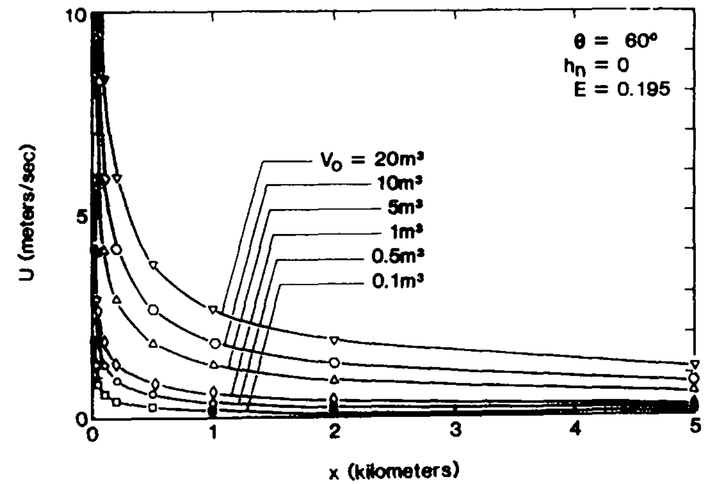

FIG. A13. Speed, U, as a function of distance, x, from virtual origin for various V_0 with $h_n = 0$, $\theta = 60°$, and $E = 0.195$.

V_0 =	0.1	0.5	1	5	10	20
x in m	U in m/sec					
10	1.87	4.18	5.91	13.20	18.67	26.41
20	1.32	2.95	4.18	9.34	13.20	18.67
50	0.84	1.87	2.64	5.91	8.35	11.81
100	0.59	1.32	1.87	4.18	5.91	8.35
200	0.42	0.93	1.32	2.95	4.18	5.91
500	0.26	0.59	0.84	1.87	2.64	3.73
1000	0.19	0.42	0.59	1.32	1.87	2.64
2000	0.13	0.30	0.42	0.93	1.32	1.87
5000	0.08	0.19	0.26	0.59	0.84	1.18

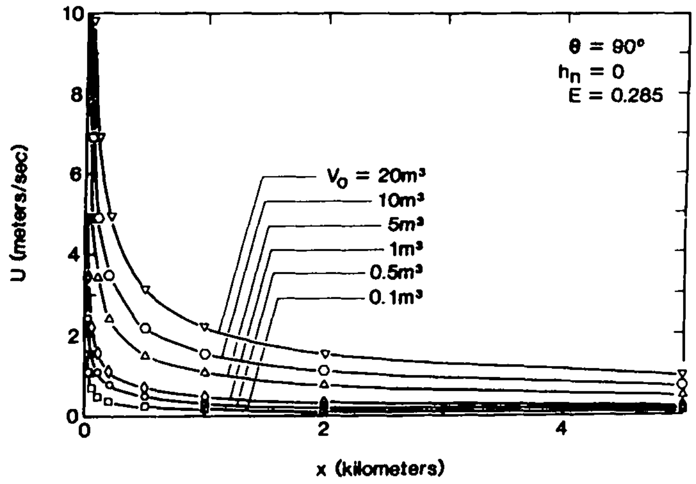

FIG. A14. Speed, U, as a function of distance, x, from virtual origin for various V_0 with $h_n = 0$, $\theta = 90°$, and $E = 0.285$.

V_0 =	0.1	0.5	1	5	10	20
x in m	U in m/sec					
10	1.54	3.45	4.88	10.92	15.45	21.84
20	1.09	2.44	3.45	7.72	10.92	15.45
50	0.69	1.54	2.18	4.88	6.91	9.77
100	0.49	1.09	1.54	3.45	4.88	6.91
200	0.35	0.77	1.09	2.44	3.45	4.88
500	0.22	0.49	0.69	1.54	2.18	3.09
1000	0.15	0.35	0.49	1.09	1.54	2.18
2000	0.11	0.24	0.35	0.77	1.09	1.54
5000	0.07	0.15	0.22	0.49	0.69	0.98